Construction and Building Materials 166 (2018) 792–807

Contents lists available at ScienceDirect

Construction and Building Materials

journal homepage: www.elsevier.com/locate/conbuildmat

Recycling trachyte waste from the quarry to the brick industry: Effects on physical and mechanical properties, and durability of new bricks

Chiara Coletti [a,*], Lara Maritan [a], Giuseppe Cultrone [b], Maria Chiara Dalconi [a], Anno Hein [c], Eduardo Molina [d,e], Claudio Mazzoli [a]

[a] Department of Geosciences, University of Padova, Via G. Gradenigo 6, 35131 Padova, Italy
[b] Department of Mineralogy and Petrology, University of Granada, Avda. Fuentenueva s/n, 18002 Granada, Spain
[c] Institute of Nanoscience and Nanotechnology, N.C.S.R. 'Demokritos', Aghia Paraskevi, 15310 Athens, Greece
[d] Centro de Excelencia en Geotermia de los Andes (CEGA, FONDAP-CONICYT), Universidad de Chile, Plaza Ercilla 803, Santiago, Chile
[e] Centro de Investigación en Nanotecnología y Materiales Avanzados, CIEN-UC, Pontificia Universidad Católica de Chile, Avenida Vicuña Mackenna 4860, Santiago, Chile

HIGHLIGHTS

- Trachyte waste represents an excellent alternative temper for brick production.
- Trachyte used as temper improves the physical and mechanical properties of bricks.
- Recycling waste may reduce requirements for raw materials currently exploited.

ARTICLE INFO

Article history:
Received 1 September 2017
Received in revised form 3 January 2018
Accepted 25 January 2018

Keywords:
Bricks
Waste recycling
Petrography
Pore system
Durability
Physical and mechanical properties

ABSTRACT

This work examined the possibility of recycling trachyte waste as temper for preparing new types of bricks, thus reducing disposal costs and requirements for increasingly vulnerable raw materials, ultimately reducing production costs. The influence of the waste addition was studied by determining the petrographic and physical characteristics of fired bricks, in order to assess their aesthetic and mechanical features. Alkali feldspars in trachyte turned out act as fluxing agents, favoring partial melting of the matrix. Textural and mineralogical analyses revealed a considerable increase in the number of connections among minerals, extensive re-crystallization of the matrix, and an overall increase in compactness, not only with increasing firing temperatures but also increasing trachyte contents. The physical and mechanical properties of all samples were comparable with those of traditional bricks, showing that the addition of trachyte confers sufficient technical features already at 900 °C, allowing further reduction of production costs by lowering firing temperatures.

1. Introduction

For millennia, clay bricks have been used as building materials, thanks to their excellent properties. From both environmental and economic perspectives, bricks are still valuable, inert and efficient construction materials. In the last few decades, extensive research has been conducted on industrial brick production, solving several environmental problems and improving sustainable development [1–8].

Improving sustainable production levels implies reduced exploitation of primary geo-resources, together with better waste management and disposal by re-assessment of residual materials as secondary resources to be used in producing new materials. Awareness of the enormous amount of waste generated by industrial processes in an age of rising environmental concerns has stimulated increasing interest in the re-use of waste and addressed research to the development of environment-friendly construction materials.

In the last few decades, many studies have examined such re-use of waste as a potential alternative to some of the primary resources used in producing bricks. Recycling organic compounds such as paper [9–12], cotton [11], tea-leaves [13], rice [14], tobacco [3], sawdust [15], biomass [16–18] and biodiesel [19] have been proposed and tested to increase brick porosity. The effect of some inorganic waste additives have been also studied, e.g. material derived from natural stone processing such as perlite [20], marble [15,21–23], pozzolana [24], fly ash [25,26], or other secondary

* Corresponding author.
E-mail address: chiara.coletti@unipd.it (C. Coletti).

https://doi.org/10.1016/j.conbuildmat.2018.01.158
0950-0618/

industrial materials such as sewage sludge [27–30], ceramic sludge [31] and leach residues [32]. Nevertheless, transfer of knowledge and technology is still very limited. Introducing waste materials into brick production may represent a sustainable solution to the problem of disposing of large volumes of substances resulting from various industrial activities, which now constitute environmental hazards worldwide [33,34]. The need to dispose of these materials and the increasing demand to develop sustainable alternatives to traditional building materials has attracted both industrial and academic attention to the production of new environment-friendly bricks [35,36] optimizing the quality of end-products and reducing their cost [37].

From this perspective, the choice of considering trachyte waste in designing a new type of brick derives from the following considerations: i) trachyte is a natural stone which does not release polluting substances or contaminants, either during firing or in use, for better environmental and social acceptance; ii) feldspars, which constitute the main mineralogical phases in trachyte, may act as fluxing agents during firing, thus improving the technical properties of bricks [38–40]; iii) recycling waste from stone processing may reduce disposal issues on one hand, and the costs of raw materials and supply on the other. This latter aspect also meets the requirements of two companies working the same industrial district (in north-east Italy), one quarrying and processing trachyte from the Euganean Hills, and the other in producing traditional bricks. In addition, re-using trachyte may represent a return to an ancient custom that of saving time and energy by taking advantage of all the possible resources of the territory, including waste materials, as attested by the ceramics produced in the course of thousands of years, from the Late Bronze Age to the Iron Age and then Roman times in north-east Italy [41–44].

The present work relies on a carefully designed multi-analytical approach to investigate the physical–mechanical properties and durability of nine brick types, obtained by adding trachyte waste to the same clayey material in order to explore new green solutions and encourage environmental-friendly brick production, sustainable use of natural resources and energy-saving processes, and promoting excellence in innovation.

2. Experimental procedure

2.1. Preparation of samples

The mix designs consist of clayey material from the alluvial plain of the Po (north Italy), known as '*Rosso Casaglia Forte*', tempered with sand-sized fragments of trachyte, mostly in the range 0.160–0.400 mm (Fig. 1a), obtained by grinding residual waste from quarrying and ornamental stone cutting.

Three types of experimental mixes were obtained by adding 5, 10 and 15 wt% of trachyte to the clayey material by means of a soft-mud process used for hand-molding. Plasticity was attained by adding water and manually working the mix, which was then placed in a 5 × 12 × 20 cm wooden mold, coated with sand to prevent the clay from sticking to the inner sides of the mold, and to favor water drainage during pressing and release. For each of the three experimental mixes fifteen samples (5 × 12 × 20 cm) were mold, five to be fired at 900 °C, five at 1000 °C and five at 1100 °C. Bricks were fired in an electric oven (Table 1) with 15 h heating time, 5 h soaking time, and 15 h cooling time (Fig. 1b).

2.2. Analytical techniques

The chemical composition of the clayey material was determined by X-ray fluorescence (XRF) on an S4 Pioneer (Bruker AXS) spectrometer, with an estimated detection limit of 0.01 wt% for

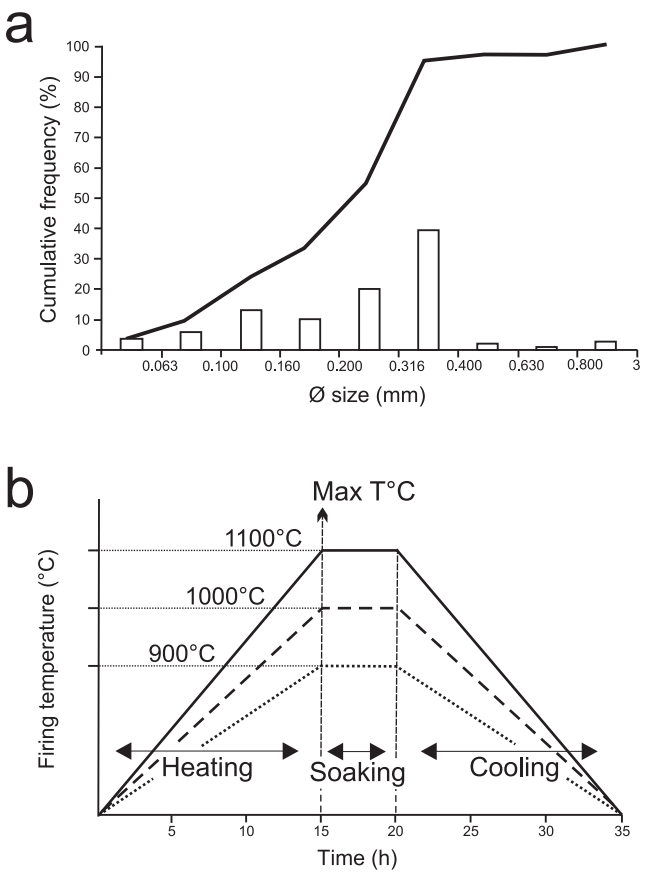

Fig. 1. a) Cumulative frequency curves of trachyte grain-size distribution; b) firing temperature vs. time.

Table 1
Trachyte waste content and firing temperature of bricks, including labels.

Raw materials		Firing temperatures (°C)		
Clay	Trachyte waste (wt%)	900	1000	1100
Rosso Casaglia Forte	5	B5.09	B5.10	B5.11
	10	B10.09	B10.10	B10.11
	15	B15.09	B10.10	B15.11

major elements; ZAF method was systematically employed [45], and the NCSDC 74301 (GSMS-1) standard [46] was used. X-ray powder diffraction (XRPD) was applied to identify the mineral phases of raw materials and fired products. Diffraction data were acquired on a PANalytical X'Pert PRO diffractometer, operating in Bragg-Brentano reflection geometry with CoKα radiation, 40 kV of voltage and 40 mA of filament current, equipped with an X'Celerator detector. Qualitative analysis of diffraction data was carried out with X'Pert HighScore Plus® software (PANalytical) and the PDF-2 database. Quantitative estimation of phase fractions (QPA) was obtained by applying the Rietveld method as implemented in Topas v4.1 software [47]. A known amount (10 wt%) of the internal standard zincite (J.T. Baker) was mixed with powdered samples of the fired bricks, in order to estimate the amorphous content according to the combined Rietveld-RIR method.

The petrographic and textural characteristics of thin sections were examined under a polarized-light optical microscope (Olympus DX-50), equipped with a Nikon D7000 digital microphotography system.

Texture and reaction microstructures were examined by Scanning Electron Microscopy (SEM) with a CamScan MX-2500

microscope, coupled with an EDAX Sapphire Si(Li) detector (LEAP + Si(Li) crystal), equipped with a LaB_6 cathode and operating at 20 kV and 160nA. Back-scattered electron images (SEM-BSE) were acquired with a resolution of 1280 × 1024 pixels. Elemental maps (512 × 400 pixels) of selected areas were acquired for several chemical elements of interest (Al, Ca, Fe, K, Mg, Na, P, Si, Ti) in order to identify reaction rims between trachyte grains and the surrounding matrix.

Water Absorption (WA) was tested on cubic samples (50 mm edge) (three samples per type of brick) [48]. Free and forced absorption (A_l and A_f), apparent and skeletal density (D_a and D_s), open porosity (P_{HT}) and degree of pore interconnection (A_x) were then calculated [49,50]. Capillary rise (B) was studied on three prism-shaped samples (25 × 25 × 120 mm) for each brick type, according to UNI EN 1925 (2000) [51]. The distribution of pore-access size (radius range: 0.001–100 μm) were determined by Mercury Intrusion Porosimetry (MIP) on a Model 9410 Micromeritics Autopore apparatus, which can generate a pressure of 414 MPa. Freshly cut samples of approximately 2 cm^3 were oven-dried for 24 h at 110 °C and then analysed. Nitrogen Adsorption (NA) determined porosity in the range 0.0002–0.15 μm (radius). The sorption isotherms were obtained at 77 K on Micromeritics Tristar 3000 apparatus. Prior to measurement, samples were heated at 130 °C for 24 h and outgassed to 10^{-3} Torr with a Micromeritics FlowPrep Degasser.

Propagation velocities Vp (compression pulse) and Vs (shear pulse) were measured by Ultrasonic Testing (UT) to determine the elastic parameters and structural anisotropy of fired bricks and to identify any variations in the degree of compactness during and after aging tests. Ultrasonic waves were transmitted in the three perpendicular directions of the cubic samples (edge: 50 mm) on a Panametrics-NDT 5058PR High Voltage pulser-receiver coupled with a Tektronix TDS 3012B oscilloscope. Measurements were performed with transducers of 1 MHz over a circular contact surface of 3 cm in diameter. A viscoelastic couplant (an ultrasound eco-gel) was used for good coupling between the transducers and the brick surfaces. Poisson's coefficient (ν), and Young (E), shear (S) and bulk (K) moduli were then calculated from measured wave velocities Vp and Vs [52], according to the apparent density values previously determined with mercury intrusion porosimetry.

The uniaxial compressive strength (UCS) test was carried out on three cubic samples (edge: 40 mm) for each brick type, on a IPEMSA S-110 press with a loading rate of 20 kg/s [53].

Thermal conductivity of disk-shaped samples (thickness: 5–7 mm; diameter: 30 mm) was determined with a steady-state hot-disk set-up according to an adapted experimental procedure [53]. The set up consisted of a brass plate with a diameter of 30 mm acting as a stabilized and monitored heat source at arbitrary temperatures up to 350 °C. The sample disk was placed on this heat source and a second cold brass plate (detector) of the same dimension was placed on the top of the sample. Measurements were taken at three heat source temperatures (c. 100, c. 200 and c. 300 °C). According to the temperature difference between the brass plates, thermal conductivity was calculated as follows:

$$k(T) = Q(T)\frac{x}{A(T_1 - T_2)}$$

in which x and A are specimen thickness and surface area of the specimen, respectively, and T_1 and T_2 are the recorded temperatures of the heating and detector plates, when steady-state had been reached. The heat flux through the sample disk Q(T) was estimated as the temperature-dependent heat loss of the detector disk to the environment, which had been determined independently. The method has proved to provide a reproducible and significant assessment of heat transmission within ceramic materials [54,55].

Resistance to salt crystallization was determined on three cubic samples (edge: 50 mm) for each brick type subjected to 10 cycles of 24 h each [56]. Frost resistance was evaluated by the freeze–thaw test on three cubic samples (edge: 50 mm) for each brick type through 30 cycles of 24 h [57]. Weight loss (ΔM/M) was calculated on samples after each cycle according to:

$$\frac{\Delta M}{M} = \frac{(W_x - W_i)}{W_i}$$

in which W_x is the weight after cycles and W_i the initial weight.

Ultrasound measurements were carried out on the brick cubes at regular intervals during the freeze–thaw and salt crystallization tests, in order to measure Vp values on the three orthogonal directions of the samples and to evaluate salt and ice damage to the pore system and texture.

The color of dried and wet fired bricks was assayed on a Konica Minolta CM-700d spectrophotometer according to the CIELab system, which describes color as lightness (L^*: −100 = black, +100 = white) and adds the two chromatic coordinates a^* and b^*, which reflect the amount of red-green and yellow-blue colors (a^*: −60 = green, +60 = red; b^*: −60 = blue, +60 = yellow), respectively. The degree of color difference (ΔE^*) was calculated according to the following equation [58]:

$$\Delta E^* = \sqrt{(L_2^* - L_1^*)^2 + (a_2^* - a_1^*)^2 + (b_2^* - b_1^*)^2}$$

where subscript '1' refers to measurements on dry samples and subscript '2' on wet ones. Measurements were carried out under a CIE standard illuminant D65 (simulating daylight with a color temperature of 6504 K) with SCI/SCE modes and wavelengths between 400 and 700 nm.

3. Results and discussion

3.1. Characterization of raw materials

The clayey material is chemically rich in SiO_2 (63.57 wt%) and Al_2O_3 (13.62 wt%), rather poor in calcium and magnesium (CaO + MgO = 6.14 wt%), and moderately rich in iron (Fe_2O_3 = 5.06 wt%) and potassium (K_2O = 2.61 wt%), with a Loss on Ignition (LOI) of 6.94 wt% (Table 2). According to XRPD analysis, quartz is the most abundant phase, followed by feldspars, associated with minor quantities of calcite, dolomite, chlorite and illite (Table 2). Trachyte waste is rich in plagioclase, quartz, K-feldspar (sanidine) and biotite. Representative XRF analyses of this trachyte are reported in Germinario et al. (2017) [59] (quarry locality: M. Altore; quarries ID 14 and 15). Under the optical microscope, trachyte shows a porphyritic texture, with phenocrysts of euhedral sanidine and plagioclase. A small amount of interstitial quartz is found among feldspar microlites in the groundmass. Biotite and widespread accessory apatite, zircon, magnetite and ilmenite were also identified. Biotite lamellae appear deformed along (001) cleavage, due to the grinding process.

3.2. Fired bricks

3.2.1. Mineralogy and texture

As all the bricks were prepared with the same raw materials but in differing proportions, they displayed similar mineralogical composition. In all cases, firing temperatures (900, 1000 and 1110 °C) exceeded those of carbonate decomposition (750 °C for dolomite, 850–900 °C for calcite) [60], and the reaction of calcium oxide with silicates of the surrounding matrix or adjacent inclusions produced new calcium-silicate phases. Chlorite and illite, found in the clayey material, started to decompose, according to Cultrone et al. (2001) [61] and Maritan et al. (2006) [62], at 600 °C and 700 °C,

Table 2
Major elements in chemical composition of clay, expressed in wt% of oxides (LOI = Lost On Ignition) and mineralogical composition of clay and temper (trachyte) determined by XRPD. Mineral abbreviations after Whitney and Evans (2010) [87]: Qz: quartz; Pl: plagioclase; Kfs: K-feldspar; Cal: calcite; Dol: dolomite; Ill: illite; Chl: chlorite; Bt: Biotite; AM: amorphous. Relative quantity: **** = very abundant; *** = abundant; ** = medium; * = scarce; – = absent.

XRF	SiO_2	Al_2O_3	Fe_2O_3	MnO	MgO	CaO	Na_2O	K_2O	TiO_2	P_2O_5	LOI
Clay	63.57	13.62	5.06	0.11	2.29	3.85	0.96	2.61	0.84	0.13	6.94

XRPD	Qz	Pl	Kfs	Cal	Dol	Ill	Chl	Bt	AM
Clay	****	***	**	**	**	*	*	–	–
Trachyte	****	**	**	–	–	–	–	*	*

respectively. Chlorite completely disappeared at 700 °C, but illite greatly decreased the intensity of its characteristic peaks in the XRPD pattern, and disappeared completely around 900 °C. The presence of calcite and illite in fired bricks, although in small quantities, up to 900 and 1000 °C (Table 3) indicated that these phases did not decompose completely. This may have been due to the large size of the crystals, the breakdown of which was limited to the rim, preserving undecomposed relics at the core [63–65], or to the semi-industrial firing procedure in an electric oven, in which heating may not have been perfectly homogeneous. Biotite derived from the trachyte temper, so that its reflections in the diffraction pattern were proportional to the abundance of trachyte in the mix, but always in small amounts (≤1 wt%) (Table 3). The peaks of illite and biotite partially overlapped in samples fired at 900 °C and 1000 °C (Fig. 2); at 1100 °C, only biotite persisted, whereas illite disappeared after complete decomposition (Fig. 2; Table 3) [61].

The diffraction patterns of the mixes showed similar behavior within the range of selected firing temperatures. The abundance of quartz remained almost unchanged (Table 3), and only slightly decreased, since quartz is involved in reactions producing new mineral phases (e.g., Ca-silicates) and increasing glass in the matrix with increasing firing temperatures [38]. Biotite and plagioclase peaks gradually decreased as those of high-temperature K-feldspar (sanidine), gehlenite and diopside, developed and progressively increased (Table 3). Cordierite (Fig. 2; Table 3) was only found in samples fired at 900 °C, probably deriving from biotite and/or chlorite decomposition and the subsequent reaction between Al-rich minerals (illite and/or feldspars of clayey materials) [62,66–68]. Gehlenite formed from the reaction between illite and calcite at 850–900 °C [69]:

(1) illite + 1.2 calcite → 0.4 K-feldspar + 0.6 gehlenite + quartz + 1.6 H_2O + 1.2 CO_2.

In the temperature range 900–1050 °C, calcium oxide derived from the decomposition of calcite (and dolomite) reacted with quartz (or free silica due to the breakdown of phyllosilicates such as chlorite and illite), forming Ca-silicates such as wollastonite [69,70], anorthite and diopside [59] (Table 3):

(2) calcite + quartz → wollastonite + CO_2;
(3) gehlenite + quartz → wollastonite + anorthite;
(4) dolomite + quartz → diopside.

The feldspars observed in the diffraction patterns of fired bricks were both relic minerals of the raw materials (mainly from the trachyte temper, but also from the clayey material) and formed during firing. The general increase in plagioclase (anorthite in Table 3) may be explained by diffusion of calcium within the Al- and Si-rich minerals constituting the raw materials (illite, biotite, quartz), the amorphous products from mineral decomposition (e.g., from chlorite) and the newly formed silicates, which also increased the amount of newly formed plagioclase, particularly anorthite (Fig. 2; Table 3). In addition, the quantity of hematite increased with firing temperature (Table 3). The amorphous phase, which also included unknown components derived from the non-stoichiometric minerals formed during sub-solidus reactions in firing, increased in content with increasing firing temperature (Table 3), but decreased with increasing trachyte content (Table 3). This was probably due to the dilution effect caused by the increasing amount of temper with respect to the matrix (i.e., pristine clayey material).

Table 3 lists the QPA results: worthy of note is the accuracy which can be attained during Rietveld quantitative phase analysis of complex polycrystalline mixtures such as the fired brick samples. The essential requirement of the Rietveld method is that the analyzed phases must be crystalline and of known structure. Any other component not described by a structural model, such as amorphous and unidentified phases, is quantified as a whole 'amorphous' fraction. In the case of crystalline phases with variable composition (e.g., minerals forming solid solutions) the requirement for known crystal structures may not be completely fulfilled, and phases with variable composition are generally described by structural models which roughly approximate their true structures.

In the fired brick samples, this occurred for feldspars and pyroxenes, both present as pristine minerals in the raw materials and/or as newly formed phases after heating. The strong peak overlapping of feldspar group minerals also hampered identification of the

Table 3
Mineralogical assemblages of fired bricks (wt%) determined by XRPD and Rietveld refinements. Tr = trachyte content (wt%). Mineral abbreviations after Whitney and Evans (2010) [87]: Qz = quartz; An = anorthite; Hem = hematite; Crd = cordierite; Ilt = illite; Cal = calcite; Gh = gehlenite; Di = diopside; Sa = sanidine; Ab = albite; Bt = biotite; AM = amorphous.

Sample	Tr (wt%)	T (°C)	Qz	An	Hem	Crd	Ilt	Cal	Gh	Di	Sa	Ab	Bt	AM
B5.09	5	900	32.5(3)	12.2(1)	0.9(1)	1.0(1)	5.2(1)	2.7(2)	3.1(1)	1.8(1)	7.0(1)	11.5(1)	<1	22(1)
B5.10		1000	32.9(3)	13.5(1)	1.2(1)	–	1.8(1)	1.6(1)	3.5(1)	4.5(1)	8.5(1)	12.6(1)	<1	20(1)
B5.11		1000	28.0(3)	16.0(2)	1.1(1)	–	–	–	2.1(1)	7.6(1)	8.0(1)	13.5(2)	<1	24(1)
B10.09	10	900	31.8(3)	26.2(3)	1.0(1)	<1	3.9(1)	2.1(1)	2.9(1)	2.9(1)	9.4(1)	11.5(1)	<1	19(1)
B10.10		1000	30.5(8)	27.7(7)	1.2(1)	–	2.1(1)	1.3(1)	3.0(1)	4.4(1)	10.0(3)	14.3(4)	<1	19(1)
B10.11		1100	25.6(3)	31.3(4)	1.2(1)	–	–	–	1.7(1)	7.0(1)	9.6(1)	12.7(1)	<1	23(1)
B15.09	15	900	28.5(3)	28.1(4)	1.8(1)	<1	5.0(1)	1.9(1)	2.1(1)	2.0(1)	11.6(1)	13.7(2)	≤1	17
B15.10		1000	28.2(3)	30.0(4)	1.2(1)	–	2.2(1)	1.6(1)	2.9(1)	3.8(4)	12.7(2)	15.2(2)	≤1	16(1)
B15.11		1000	25.9(3)	32.0(4)	2.4(1)	–	–	–	2.0(1)	6.5(1)	11.8(2)	15.7(2)	≤1	19(1)

Phase weight fractions and esd's, in parentheses, as computed by Topas.

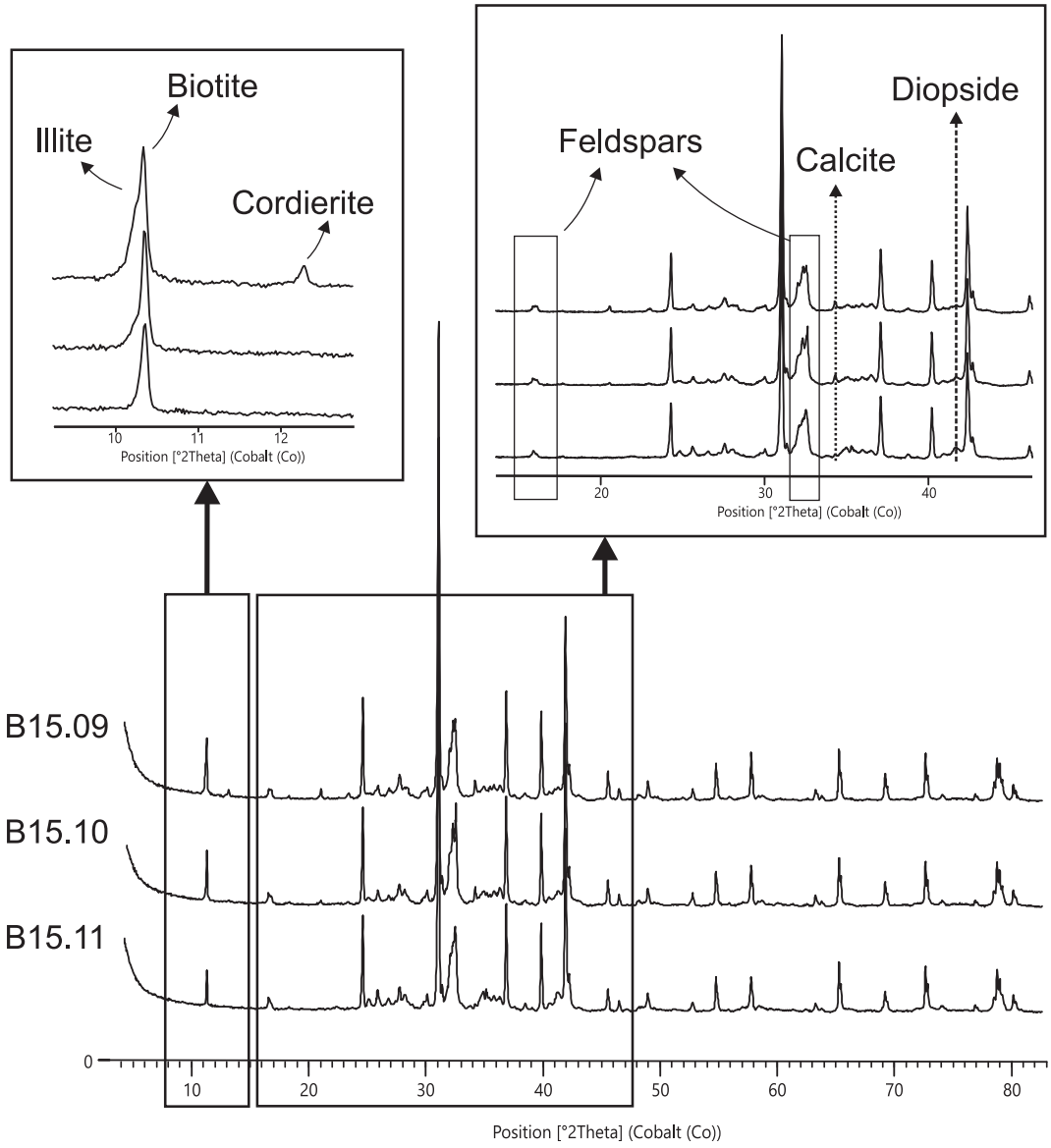

Fig. 2. Comparison between XRPD patterns of three bricks obtained from mixed design with 15 wt% trachyte and fired at 900, 1000 and 1100 °C, respectively.

correct mineral composition of the feldspar mixture in the sample. During Rietveld refinement of the fired bricks, the feldspar components were described according to the structural models of sanidine (ICSD#90141), albite (ICSD#16744) and anorthite sodian (ICSD#100234), kept constant for all analyzed samples. This is clearly an approximation of the true feldspar compositions, which were expected to change slightly during heating. Similarly, pyroxenes of variable composition formed during heating were approximated by a diopside structural model (ICSD#30522). Within this approximation, QPA results showed significant increases in anorthite and pyroxene with increasing firing temperatures; the increase in the sanidine weight fraction was not great. It should be noted that the ESDs listed in Table 3 are only related to the mathematical fit of the refinement and do not represent errors in the final quantification. A more realistic estimate of errors in the QPA of complex mixtures with phases described by approximated structural models indicated relative errors as large as 20–30% [71].

Trachyte grains were evident under the optical microscope (Fig. 3a), and often contained lamellae of biotite, also dispersed in the matrix of the brick as isolated flakes (Fig. 3c, e). Under reflected light (Fig. 3b, d, f), a thick rim appeared, formed of symplectite K-feldspar, spinel and magnetite. This reaction microstructure developed during magma ascent and dehydration, and was similar to the crustal xenoliths which underwent pyrometamorphism after incorporation in the Euganean trachyte [72] and crystallized during the formation of trachyte, when changing temperatures, pressures and other physical conditions (e.g., fluid composition or activity), recrystallized unstable phases to more stable constituents.

Biotite preserved its typical pleochroism (Fig. 3g, h) in the fired bricks; opaque anhedral and euhedral Fe-Ti oxide minerals were also quite common (Fig. 3i, j).

Scanning electron microscope analysis of fired samples showed progressive changes in the texture of bricks as firing temperature increased. Bricks fired at 900 °C had irregularly shaped pores and grains poorly connected with the surrounding matrix (Fig. 4a, b), whereas those fired at 1000 °C and 1100 °C showed increasingly pronounced vitrification and pore-shape homogenization and roundness. The same effect was seen with increasing trachyte content. As an example, similar textural features were observed in

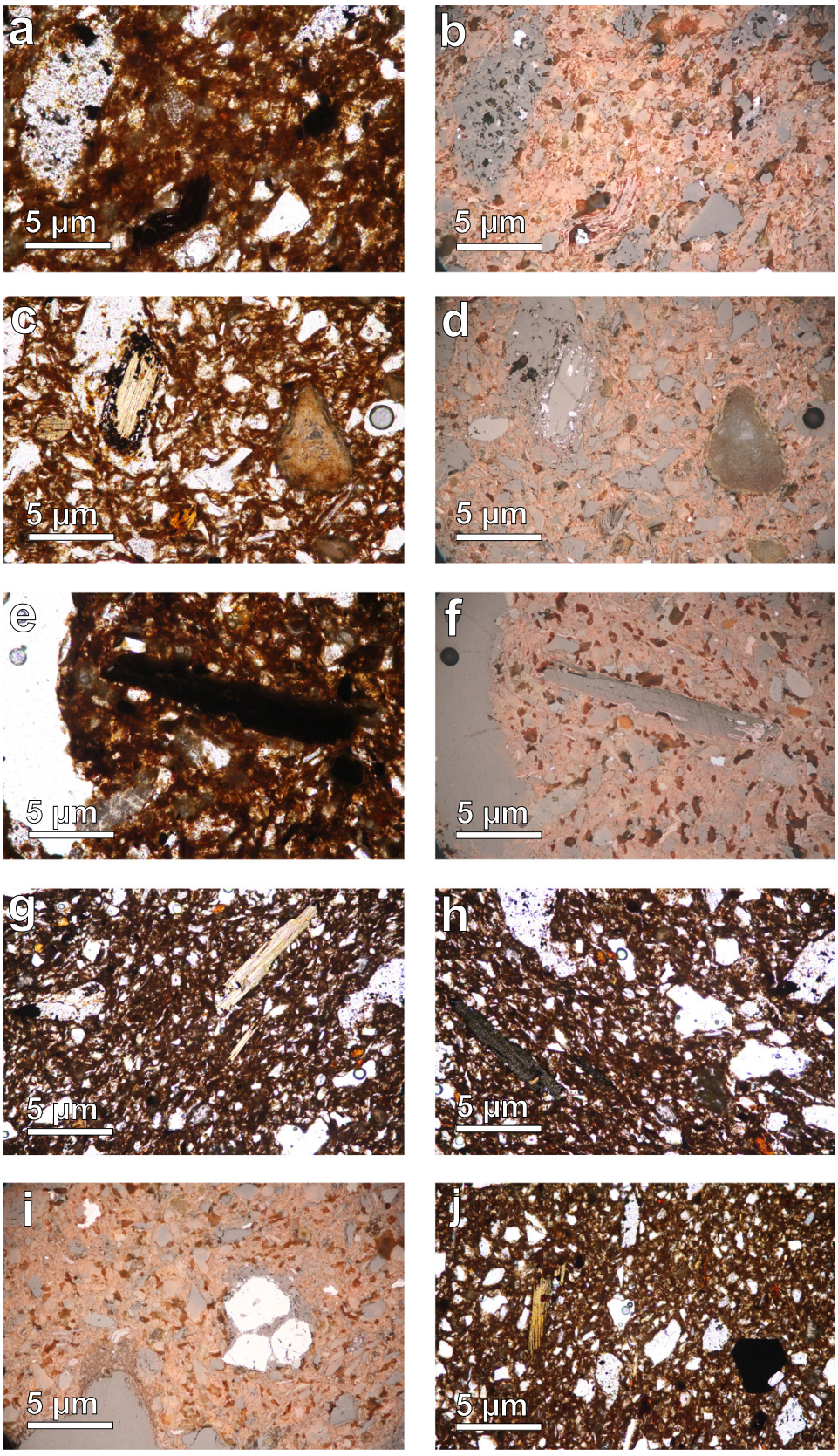

Fig. 3. Photomicrographs in transmitted plane-polarized light (PPL) and reflected light (RL) of fired bricks: (a-b) Trachyte grains and biotite in brick B15.11 (PPL and RL images, respectively); (c-d) biotite flake characterized by symplectitic rims in brick B5.09 (PPL and RL images); (e-f) biotite flake in brick B10.11 (PPL and RL images); (g-h) biotite pleochroism at two angular positions (brick B15.09; PPL); (i-j) opaque minerals (Fe-Ti oxides) (in brick B15.09 in RL; in brick B10.09 in PPL).

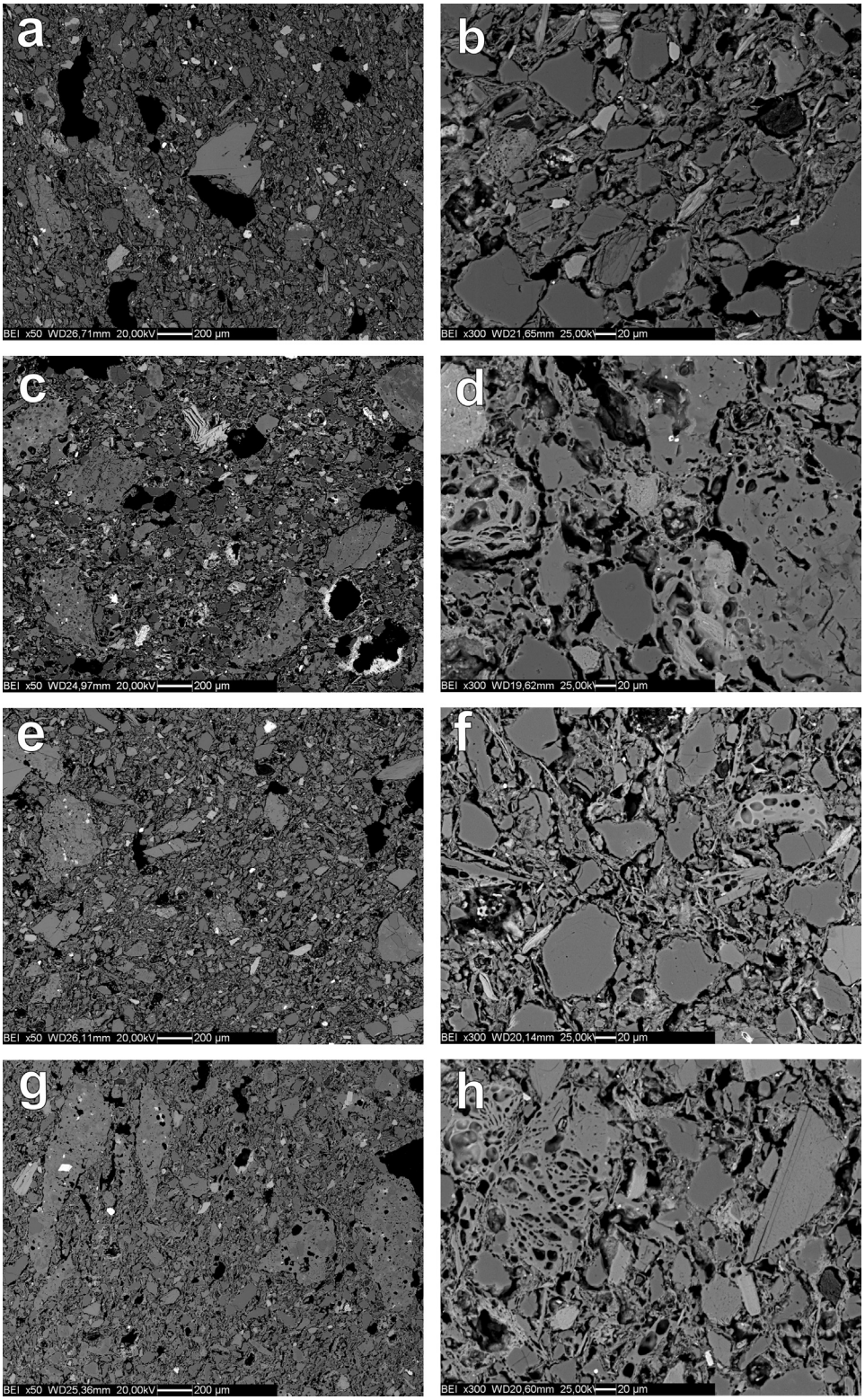

Fig. 4. SEM-BSE images of textural evolution as function of firing temperature and trachyte content: a-b) brick B5.09; c-d) brick B5.11; e-f) brick B10.10; g-h) brick B15.11.

bricks containing 5 wt% of trachyte and fired at 1100 °C (Fig. 4c, d) and in ones containing 10 wt% of trachyte and fired at 1000 °C (Fig. 4e, f). With higher trachyte concentration (15 wt%), the groundmass was extremely compact in samples fired at 1100 °C, showing grains firmly bonded to the surrounding matrix by glass bridges (Fig. 4g, h).

Vitrification preferentially occurred along trachyte grain boundaries and domains occupied by the amorphous phase generated during firing, when characteristic high-temperature vesicles developed (Fig. 5a). The distribution map of K (Fig. 5b) shows that its contents in the amorphous phase decreased from trachyte grains toward the surrounding matrix, indicating outward diffusion from

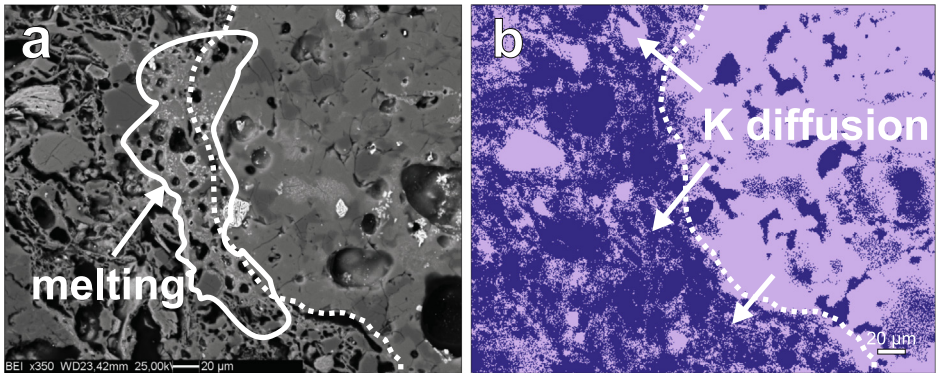

Fig. 5. a) Fluxing effect of trachyte (brick B10.11); b) detail of K elemental map around a trachyte grain, indicating outward diffusion of element.

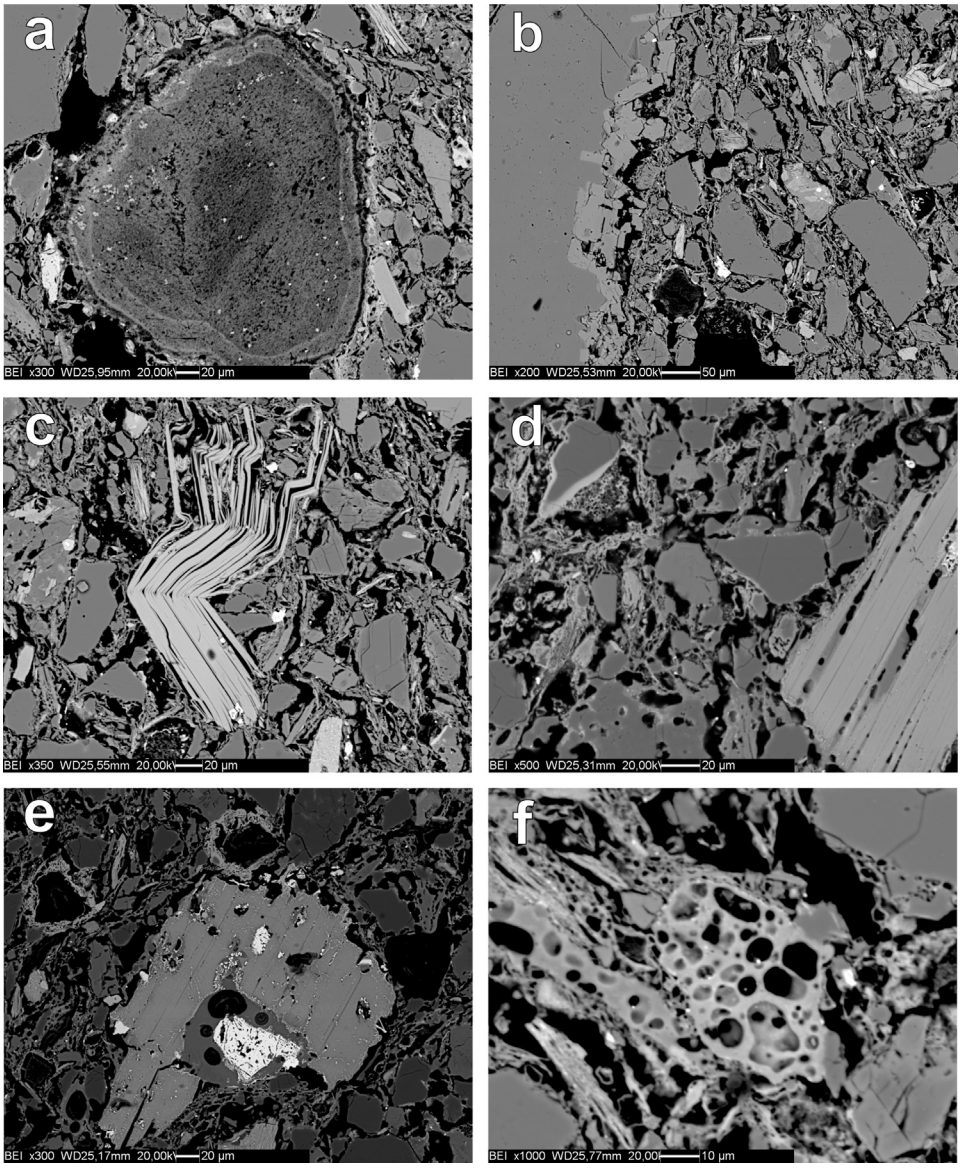

Fig. 6. a) Calcite grain, after partial reaction with surrounding matrix and recrystallized after decarbonation (brick B10.10); b) euhedral gehlenite crystals growing along a quartz rim (brick B5.10); c) flake of dehydroxylated biotite (brick B10.09); d) reaction rims between grains and surrounding matrix; biotite flake with typical alteration along (001) cleavage planes and development of secondary porosity (brick B15.11); e) illite flake partially reacted with surrounding matrix (brick B5.11); f) bubbles developed in a vitrified portion of matrix (brick B5.10).

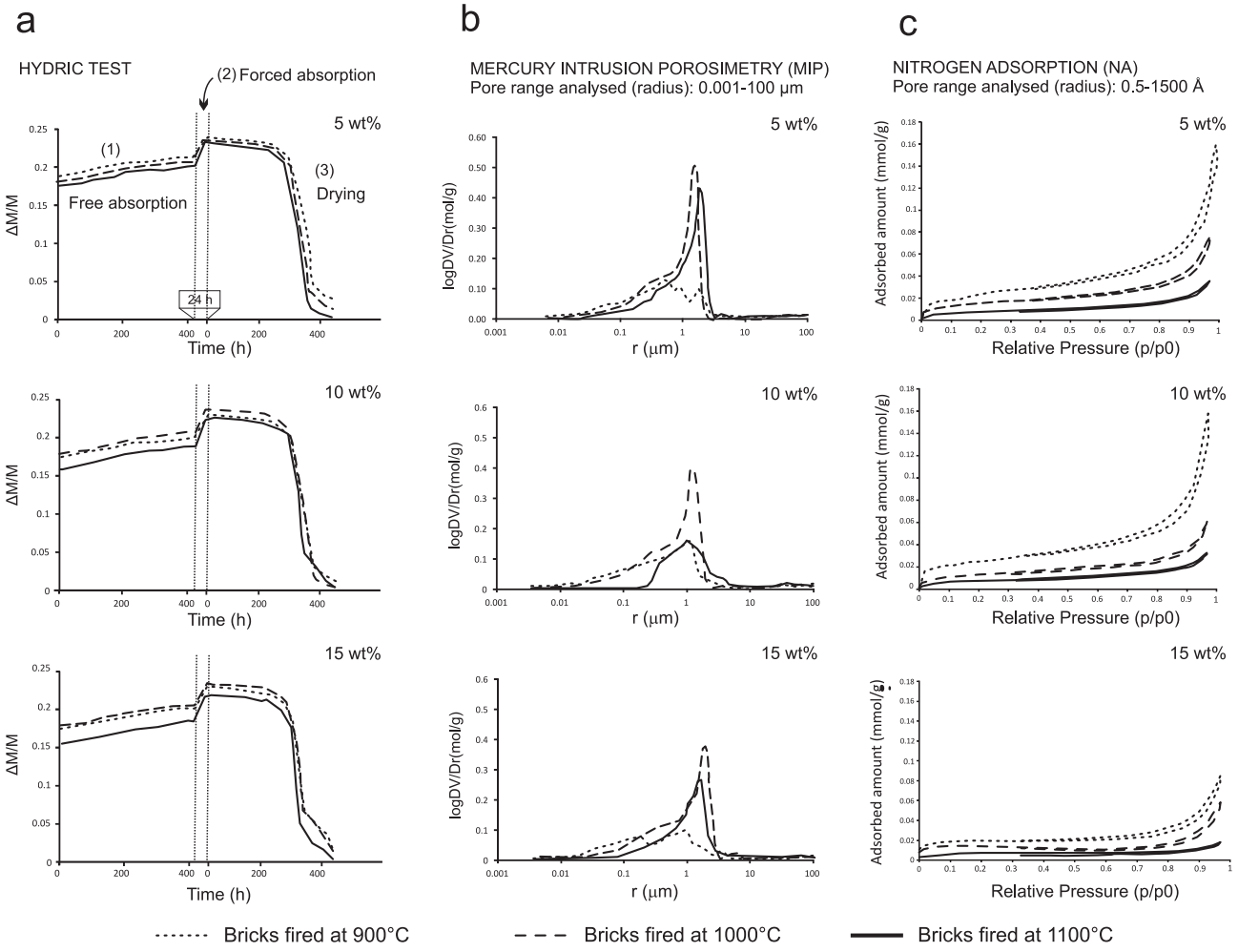

Fig. 7. a) Results of hydric test, expressed as weight variation (ΔM/M) vs. time (h): free water absorption (1), forced water absorption (2), drying (3) of fired bricks; b) Mercury Intrusion Porosimetry curves, c) N_2 adsorption–desorption isotherms. Samples grouped according to percentage of trachyte added: top 5 wt%, middle 10 wt%, bottom 15 wt%.

Table 4
Hydric Test (HT): A_I = free water absorption; A_f = forced water absorption; A_x = degree of pore interconnection; S = saturation coefficient; P_{HT} = open porosity; D_a = apparent density; D_s = skeletal density. B = capillarity rise (measured after 9 min). Mercury Intrusion Porosimetry (MIP): P_{MIP} = open porosity; d_b = bulk density; d_{sk} = skeletal density. Nitrogen Adsorption (NA): Sa = surface area.

		B5.09	B5.10	B5.11	B10.09	B10.10	B10.11	B15.09	B15.10	B15.11
Tr (wt%)		5			10			15		
T(°C)		900	1000	1100	900	1000	1100	900	1000	1100
Hydric test (HT)	A_I (%)	21.19	20.73	20.21	19.72	20.30	18.56	19.82	20.14	17.98
	A_f (%)	23.52	23.33	22.99	22.29	23.16	21.97	22.26	22.77	21.16
	A_x (%)	9.91	11.16	12.12	11.55	12.35	15.52	10.97	11.53	15.06
	S (%)	61.28	59.95	59.39	57.17	59.82	56.86	57.37	58.65	54.73
	P_{HT} (%)	37.90	37.48	37.26	36.37	37.43	36.25	36.46	36.96	35.37
	D_a (g/cm^3)	1.61	1.61	1.62	1.63	1.62	1.65	1.64	1.62	1.67
	D_s (g/cm^3)	2.60	2.57	2.58	2.56	2.58	2.59	2.58	2.58	2.59
	B (cm/$\sqrt{t}$)	0.04	0.06	0.06	0.04	0.06	0.07	0.04	0.06	0.07
Mercury intrusion porosimetry (MIP)	P_{MIP} (%)	25.23	38.17	34.47	27.56	38.40	19.40	23.22	36.96	27.58
	d_b (g/cm^3)	1.56	1.59	1.65	1.57	1.58	1.61	1.64	1.60	1.67
	d_{sk} (g/cm^3)	2.09	2.57	2.52	2.17	2.56	2.01	2.13	2.54	2.31
Nitrogen adsorption (NA)	Sa (m^2/g)	2.1143	1.2133	0.6265	1.9301	0.9788	0.5832	1.4759	0.9541	0.5002

the feldspar contained in the trachyte. Potassium acted as fluxing agent in the mix, since the groundmass surrounding trachyte grains, enriched in K, was also more compact. The effect of feldspars is well-known, as they are widely used for fluxing and bonding matrices and grains in ceramic materials [73]. They cause the mix to melt gradually over a wider thermal interval, favoring sintering of quartz and clay minerals, and lowering the temperature of the glassy phase formation. In particular, the sintering point of

Table 5
Ultrasonic test (UT): Vp = compressional propagation velocity of ultrasonic pulses; Vs = shear propagation velocity of ultrasonic pulses; Δm = Relative anisotropy; ν = Poisson's ratio; E = Young's modulus; G = shear modulus; K = bulk modulus. UCS = uniaxial compressive strength test: σ = mechanical stress.

Sample		B5.09	B5.10	B5.11	B10.09	B10.10	B10.11	B15.09	B15.10	B15.11
Tr (wt%)		5			10			15		
T(°C)		900	1000	1100	900	1000	1100	900	1000	1100
UT	Vp (m s^{-1})	2230	2071	2263	2087	1845	2228	2100	1972	2148
	Vs (m s^{-1})	1276	1074	1187	1047	952	1140	1086	1024	1126
	Δm	8.52	12.64	5.00	9.21	10.93	7.07	12.31	10.24	7.78
	ν	0.26	0.32	0.31	0.33	0.33	0.32	0.32	0.32	0.31
	E (GPa)	6.38	4.83	6.09	4.58	3.80	5.53	5.10	4.41	5.55
	G (GPa)	2.54	1.83	2.32	1.72	1.43	2.09	1.93	1.68	2.12
	K (GPa)	4.37	4.37	5.35	4.54	3.65	5.20	4.65	3.99	4.88
UCS	σ (kg/cm^2)	65	–	91	80	86	117	75	92	122

plagioclase is around 1000 °C [40,74], whereas sanidine has an incongruent melting temperature of about 1050 °C [75].

As regards other types of inclusions naturally occurring in the clay, at 1000 °C calcite grains only partially reacted with the surrounding matrix, forming reaction rims (Fig. 6a). The occurrence of calcite at this relatively high temperature was also confirmed by XRPD data. The high diffusion of Ca and Mg ions in the groundmass and the reaction with quartz and feldspar grains led to the formation of wollastonite, diopside and gehlenite (Fig. 6b). At 900 °C, biotite was partially dehydroxylated (Fig. 6c) and at 1000 °C it showed typical alterations along (001) cleavage planes, with the development of secondary porosity (Fig. 6d), whereas quartz grains showed coronas and resorption forms. At 1100 °C, illite decomposed completely, with Fe-bearing oxides crystallizing along grain boundaries and cleavage planes, and forming glass patches with vesicles (Fig. 6e). Rounded pores were also quite frequent in the glassy matrix at 1100 °C (Fig. 6f).

3.2.2. Porosity

Water absorption decreased with increasing trachyte contents and firing temperature (Fig. 7a). Both trachyte contents and firing temperature contributed to modifying the pore system in bricks. Samples containing 5 wt% of trachyte recorded a quite small but significant decrease in absorption at increasing temperatures. Reduced absorption as a function of firing temperature was more pronounced with higher trachyte contents, samples containing 15 wt% of trachyte and fired at 1100 °C showing the lowest water absorption values (Fig. 7a; Table 4).

Changes in the pore system were also confirmed by the degree of pore interconnections (A_x) which generally increased with increasing firing temperature and trachyte contents (Table 4). Similarly, the saturation coefficient (S) decreased with increasing temperature and trachyte contents.

Hydric parameters (Table 4) indicated decrease in open porosity, giving rise to an increase in apparent density (D_a) as temperature and trachyte contents rose. This indicated the formation of a more compact material, due to the combined effect of higher firing temperature and increased quantity of trachyte, acting as fluxing agent (Fig. 5a), although the small variations in skeletal density (D_s), which slightly decreased at increasing temperature only in samples with 5 wt% of trachyte, indicated a progressive increase in closed pores, congruent with petrographic observations.

Similar trends were inferred from MIP, when open porosity increased in bricks fired at 1000 °C and decreased in those fired at 1100 °C, while bulk density (d_b) increased with firing temperatures. According to porosimetric curves, small pores prevailed in samples fired at 900 °C, whereas dispersion in frequency distribution patterns became narrower and peaks shifted towards larger pores (1–10 μm) with increasing temperatures (Fig. 7b).

The presence of larger pores in bricks fired at higher temperatures was also confirmed by the behavior of water in the capillary rise test: here, the highest rise, after 9 min (B), was observed in samples fired at 1100 °C (Table 4). Capillary rise also increased with trachyte content, as expected, in view of its fluxing effect. During sintering, the morphology and size of pores were both modified, becoming larger and reducing interconnectivity [76,77]. These features were also confirmed by the Nitrogen adsorption Type IV isotherms characterized by hysteresis (according to the IUPAC classification) [78,79], typical of materials in which mesopores prevail (Fig. 7c) and the gradual reduction in surface area (S_a) (Table 4), congruent with textural features (Figs. 4 and 5) and the significance of the A_x values, discussed above.

3.2.3. Physical and mechanical properties

Bricks fired at 1100 °C displayed higher Vp (compression pulse) and Vs (shear pulse) velocities and lower relative anisotropy (Δm). This indicated that they were the most compact products, characterized by elevated particle bonding, lower porosity, and higher textural homogeneity. The Poisson ratio (ν) was very similar in all bricks except B5.09, which had the lowest values (Table 5). Young (E), shear (G) and bulk (K) moduli were quite variable, due to the contrasting effect of glass, the amount of which was proportional to firing temperature and content in trachyte temper. Tempered grains tended to reduce wave transmission by multiple reflections and refractions [80]. Consistently, samples with the lowest velocity values were those with 10 wt% of trachyte fired at 1000 °C, which were characterized by low vitrification. Instead, the mix with only 5 wt% of trachyte provided bricks with higher matrix homogeneity, favoring wave transmission despite low vitrification (Table 5). Other bricks fired at 1000 °C had larger pores, as confirmed by their high free absorption (A_l) in the hydric test (Fig. 7a; Table 4) and their open porosity, as determined by MIP (Fig. 7b), which are additional obstacles to the transmission of ultrasonic waves.

However, the uniaxial compression test showed a linear increase in strength with increasing firing temperature and trachyte contents (Table 5). The improved strength of the ceramic body was caused by the feldspars in trachyte grains, which favor partial melting, locally cementing crystalline phases in the matrix.

Analysis of thermal conductivity showed various kinds of behavior, according to brick type (Table 6). Samples with 5 wt% of trachyte had lower thermal conductivity values than those observed in samples with higher contents. With firing temperature increasing from 900 °C to 1100 °C, thermal conductivity slightly increased or remained stable. Instead, samples with 10 wt% and 15 wt% of trachyte had higher thermal conductivity, which clearly decreased with increasing firing temperature. All samples fired at 1100 °C recorded similar values of thermal conductivity, regardless of their trachyte content. Anisotropy in samples containing 5 wt%

Table 6
Effective thermal conductivity (k_{eff}) measured parallel (p) and normal (n) to base of fired bricks. Corrected values determined form measured ones accounting for effective area of samples. Also shown: average values (ave) of k_{eff}, geometric parameters, weight and density of samples. Anisotropy (An) calculated as $|1 - (k_{eff(p)}/k_{eff(n)})|$, i.e., value becomes zero when sample is isotropic.

Sample		Dimension/weight/density					Measured values												Effective area	Corrected values								
		Thickness [mm]	Diameter [mm]	Weight [gr]	Volume [cm^3]	Density [g/cm^3]	T_1 (°C)	T_2 (°C)	Loss	k	T_1 (°C)	T_2 (°C)	Loss	k	T_1 (°C)	T_2 (°C)	Loss	k		k_{eff} (~100 °C)	ave	An	k_{eff} (~200 °C)	ave	An	k_{eff} (~300 °C)	ave	An
B5.09	n	4.96	29.38	5.93	3.363	1.76	119.0	100.5	−2.71	1.07	220.7	174.9	−6.24	1.00	315.7	238.0	−10.15	0.96	1.00	1.07	1.13	0.11	1.00	1.02	0.06	0.96	0.99	0.08
	p	7.96	29.56	9.40	5.463	1.72	119.7	94.6	−2.47	1.14	219.3	157.9	−5.35	1.01	315.2	214.3	−8.60	0.99	0.96	1.19			1.05			1.03		
B5.10	n	4.66	29.42	5.37	3.168	1.70	121.5	106.0	−2.87	1.27	227.8	186.2	−6.74	1.11	323.7	253.6	−11.13	1.09	0.99	1.28	1.26	0.04	1.12	1.12	0.01	1.10	1.07	0.05
	p	6.52	29.62	7.54	4.493	1.68	122.2	100.1	−2.74	1.17	224.6	170.4	−6.07	1.06	320.8	228.8	−9.60	0.99	0.95	1.23			1.12			1.04		
B5.11	n	5.14	29.34	6.18	3.475	1.78	120.0	102.7	−2.76	1.21	225.9	180.4	−6.50	1.09	320.9	245.5	−10.57	1.07	0.98	1.24	1.17	0.11	1.11	1.07	0.07	1.09	1.03	0.10
	p	6.04	29.56	7.53	4.145	1.82	119.7	98.7	−2.63	1.10	225.0	172.9	−6.12	1.03	320.2	232.7	−9.73	0.98	1.00	1.10			1.03			0.98		
B10.09	n	5.16	29.28	6.31	3.474	1.82	121.5	105.5	−2.88	1.38	225.6	184.4	−6.72	1.25	320.9	251.3	−10.96	1.21	0.97	1.42	1.27	0.21	1.29	1.12	0.26	1.24	1.08	0.26
	p	6.70	29.52	8.19	4.586	1.79	122.3	99.2	−2.66	1.13	223.1	165.5	−5.59	0.95	324.2	226.9	−9.13	0.92	1.00	1.13			0.95			0.92		
B10.10	n	6.00	29.20	6.95	4.018	1.73	123.0	100.3	−2.69	1.06	228.9	173.7	−6.18	1.00	325.0	234.4	−9.88	0.98	0.94	1.13	1.26	0.22	1.07	1.18	0.21	1.04	1.10	0.12
	p	3.68	29.50	4.41	2.515	1.75	117.8	106.5	−2.90	1.38	219.6	190.3	−7.04	1.29	313.0	259.7	−11.57	1.17	1.00	1.38			1.29			1.17		
B10.11	n	6.64	29.22	7.83	4.453	1.76	122.5	102.3	−2.59	1.27	228.2	176.2	−6.03	1.15	324.8	238.4	−9.69	1.11	0.99	1.28	1.34	0.09	1.16	1.15	0.02	1.12	1.10	0.04
	p	6.10	29.44	7.20	4.152	1.73	123.5	104.2	−2.94	1.37	227.4	176.3	−6.37	1.12	326.1	239.2	−10.25	1.06	0.98	1.39			1.14			1.08		
B15.09	n	5.40	29.54	6.44	3.701	1.74	122.6	104.7	−2.97	1.31	222.7	176.4	−6.42	1.09	319.0	241.0	−10.41	1.05	0.94	1.39	1.20	0.28	1.16	1.06	0.17	1.12	1.03	0.16
	p	7.36	29.22	8.53	4.935	1.73	121.7	95.1	−2.44	1.01	228.3	164.1	−5.61	0.96	324.2	220.5	−8.89	0.94	1.00	1.01			0.96			0.94		
B15.10	n	3.70	29.60	4.34	2.546	1.70	122.5	107.1	−2.90	1.01	225.7	186.8	−6.67	0.92	326.0	260.1	−11.21	0.91	1.00	1.01	1.22	0.42	0.92	1.08	0.34	0.91	1.05	0.29
	p	6.96	29.76	8.19	4.841	1.69	121.7	101.6	−2.80	1.39	223.3	172.0	−6.14	1.20	321.2	234.2	−9.94	1.14	0.97	1.44			1.23			1.18		
B15.11	n	6.08	29.70	7.02	4.212	1.67	121.5	99.2	−2.65	1.04	226.5	171.9	−6.06	0.97	322.5	233.9	−9.87	0.98	0.96	1.09	1.06	0.05	1.01	0.99	0.05	1.02	0.98	0.08
	p	6.40	29.80	7.53	4.464	1.69	120.5	97.8	−2.54	1.03	226.4	170.2	−5.92	0.97	323.5	229.9	−9.52	0.93	1.00	1.03			0.97			0.93		

of trachyte was always low at all firing temperatures. Samples containing higher amounts of trachyte showed strong anisotropy of thermal conductivity when fired at 900 °C. At increasing temperatures, anisotropy gradually decreased up to firing temperatures of 1100 °C [55]. The general reduction in porosity with increasing trachyte content led to greater thermal conductivity as trachyte content increased. The rise in anisotropy with trachyte content indicates that trachyte fragments are generally anisotropic and tend to become oriented in the mix during sample forming, although not systematically with respect to specific brick surfaces, as higher thermal conductivity has sometimes been recorded parallel and at others normal to the base of the brick. The presence of trachyte in the mix favors vitrification during firing, with a reduction in open porosity with increasing temperatures.

Further temperature increases favor the growth of vesicles in the vitrified portions, increasing the number of closed pores. At 1100 °C, textural inhomogeneity is due to the presence of large pores and inclusions, both acting as barriers [54,81], which modify the heating flux and compromise homogeneous distribution of heat. This is congruent with the initial slight increase in thermal conductivity from 900 °C to 1000 °C, which is more pronounced at higher trachyte contents, and the subsequent reduction of thermal conductivity [82]. It also explains the progressive reduction of anisotropy, which almost disappears at 1100 °C.

Comparisons between pore-size distribution and physical properties revealed substantial changes in texture. Total open porosity as investigated by free water absorption and MIP (range 0.1–100 μm) displayed non-linear behavior: instead of changing progressively with increasing temperature [76], porosity initially increased and then decreased. Conversely, the number of small pores measured with NA (radius < 1500 Å) gradually diminished (Fig. 7c), and that of pores measured with MIP in the range 1–10 μm increased with increasing temperature. This effect was confirmed by the high capillarity rise (B) of bricks fired at 1100 °C [83]. The observed changes in porosity with temperature, the linear increases in density, compactness (σ) and capillarity (B), and reduced interconnections may all be explained by the increasing sintering effect between 1000 °C and 1100 °C. Principal Component Analysis (PCA) (Fig. 8a) of the main physical and mechanical properties showed that thermal conductivity better discriminated bricks fired at 900 °C, despite their different trachyte contents. Instead, open porosity, as shown by both MIP and the hydric test, better identified samples fired at 1000 °C. In addition, brick B5.11 tended to cluster with this group. This sample was characterized by a large number of pores larger than 10 μm, which are poorly detected by MIP due to instrumental limitation [84] and which persist at high temperature, since sintering may not be sufficiently pervasive [85,86]. Other physical and mechanical properties such as mechanical resistance, ultrasound velocity, bulk density and porosity in the radius range 1–10 μm mainly affected the behavior of bricks fired at 1100 °C. The gradual increase in the melted fraction with increasing firing temperature, especially in bricks with high trachyte content (10 and 15 wt%), made the ceramic structure more compact, and minerals and rock fragments were progressively embedded into and welded by a partially melted matrix [77].

The dendrogram from hierarchical cluster analysis on the same physical and mechanical properties (Fig. 8b) showed that samples fired at 900 °C formed a cluster (*cluster 1*) separate from that of samples fired at 1000 °C (*cluster 2*), indicating that firing temperature had a definite effect on physical and mechanical properties, with respect to the amount of trachyte added. The fluxing action of trachyte increased with rising temperatures. Although brick B5.11 (fired at 1100 °C) fell in cluster 2, together with samples fired at 1000 °C, bricks B10.11 and B15.11 displayed a greater degree of dissimilarity.

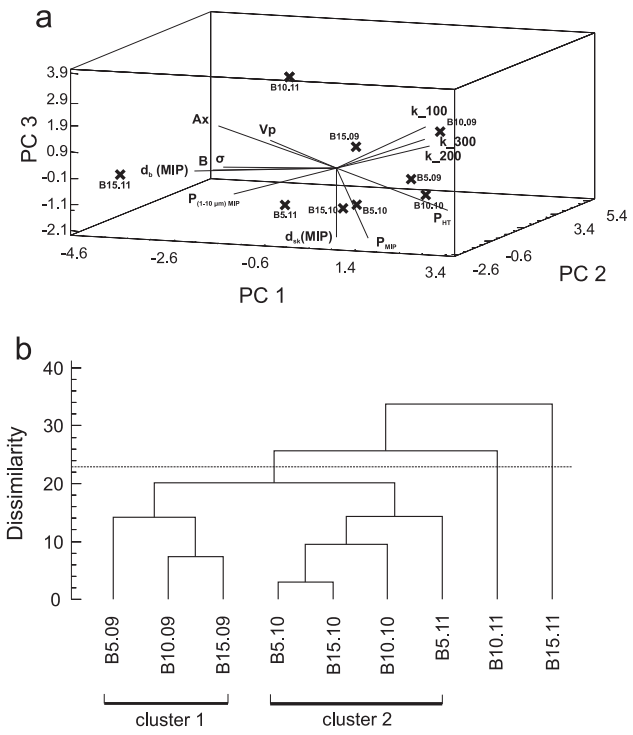

Fig. 8. a) Scores and loading plots of PCA on following variables: P_{HT} = open porosity (%); P_{MIP} = open porosity (%); k_100 = thermal conductivity at ~100 °C (W m^{-1} K^{-1}); k_200 = thermal conductivity at ~200 °C (W m^{-1} K^{-1}); k_300 = thermal conductivity at ~300 °C (W m^{-1} K^{-1}); d_b (MIP) = bulk density (g cm^{-3}); d_{sk} (MIP) = skeletal density (g cm^{-3}); A_x = pore interconnection (%); Vp = compressional propagation velocity of ultrasonic pulses (m s^{-1}); B = capillarity rise (cm/$\sqrt{t}$); σ = mechanical stress in uniaxial compressive test (kg cm^{-2}); $P_{(1-10\ \mu m)\ MIP}$ = open porosity with radius 1–10 μm (%). PC1, PC2 and PC3: 35%, 28% and 20% (total 83%) of total variance, respectively; b) dendrogram of cluster analysis according to average linkage method and square Euclidean distance performed on the variables used for the PCA.

3.2.4. Durability

After salt crystallization (Fig. 9a) and freeze–thaw (Fig. 9b) testing, bricks fired at higher temperature (1100 °C) displayed slightly greater durability than those fired at lower temperature (900 °C; 1000 °C). Damage after accelerated aging tests was visually limited and confined mainly to the edges and vertices of cubic samples, with little loss of material. In the case of salt crystallization, the weight change after testing recorded a slight increase from 1 to 6 wt% for all bricks (Fig. 9a), indicating that a small amount of salt remained within the pores, despite repeated cycles of distilled water bathing at the end of the test. The precipitation of salt in the brick pores also led to increased ultrasonic wave velocity during salt crystallization cycles (Fig. 10a). Weight loss turned out to be extremely limited after freeze–thaw cycles, with further decreases at increasing firing temperatures; therefore, all bricks showed very strong resistance to this stress condition (Fig. 9b). The lack of ultrasonic wave transmission after 20 and 25 freeze–thaw cycles in bricks B5.11 and B10.09 (Fig. 10b), respectively, indicated that some changes occurred at textural level, despite the absence of macroscopic evidence of damage or weight loss. Microcracks and fissures probably developed in these bricks, hindering ultrasonic wave transmission.

3.2.5. Color

The potential introduction of these materials to the market also requires analysis of aesthetic aspects, i.e., color and its possible variability in conditions of use.

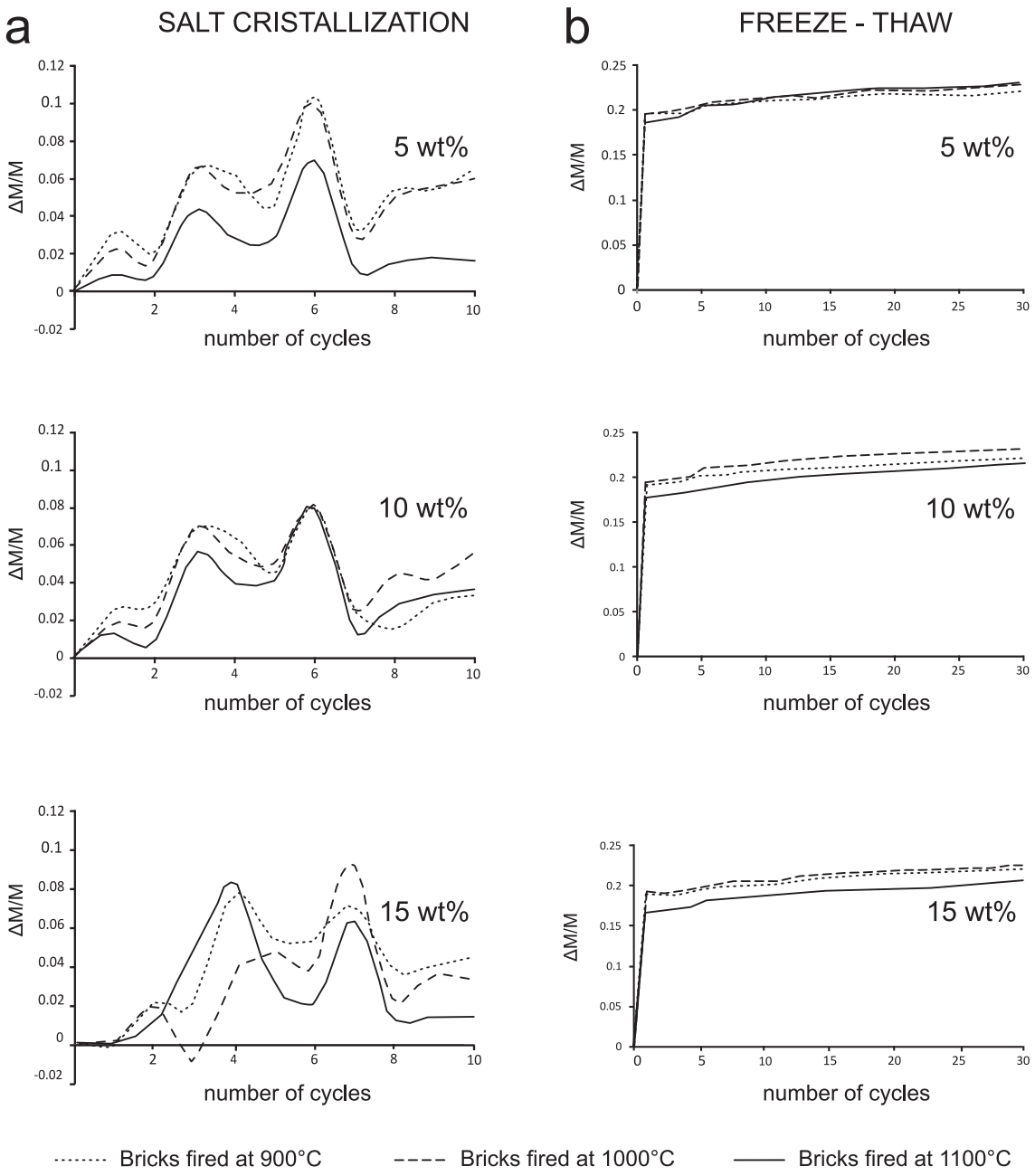

Fig. 9. a) Weight variation (ΔM/M) vs. number of salt crystallization cycles on bricks; b) weight variation (ΔM/M) vs. number of freeze-thaw cycles on bricks.

A general decrease in chromatic coordinates (a^* and b^*) and lightness (L^*) with increasing firing temperature was observed in both dry and wet samples (Table 7). Bricks fired at 900 °C and 1000 °C overlapped in the a^*b^* space, in the field of a yellow-red hue, whereas those fired at 1100 °C were located closer to the origin, toward the field of grayish colors. a^* and L^* were the color components most affected by changes due to increased trachyte content (Fig. 11; Table 7).

Differences among samples were more evident when dry-wet color changes (ΔE) were examined. This feature was less pronounced in samples with higher trachyte content (brick B15.11: ΔE = 11.26), which means that, in wet conditions (e.g., exposed to rain) bricks with 15 wt% of trachyte are less subject to color change. However, the contribution of trachyte itself to the color was quite low. This is an important point when considering the aesthetic features of bricks, indicating that a considerable fraction of trachyte can be added to the clayey material without substantial changes in the final aspect of the fired product.

4. Conclusions

Characterization of the physical and mechanical properties of these bricks, and of their durability and color clearly show the effects of trachyte waste as temper in brick production:

- physical and mechanical properties improve with both increases in firing temperature and trachyte content, together with significant changes in brick texture, i.e., increased numbers of connections among grains with increasing amount of glass, and reduction of anisotropy;
- water absorption decreases with increasing trachyte content, as an effect of the overall reduction in pore interconnections (A_x);

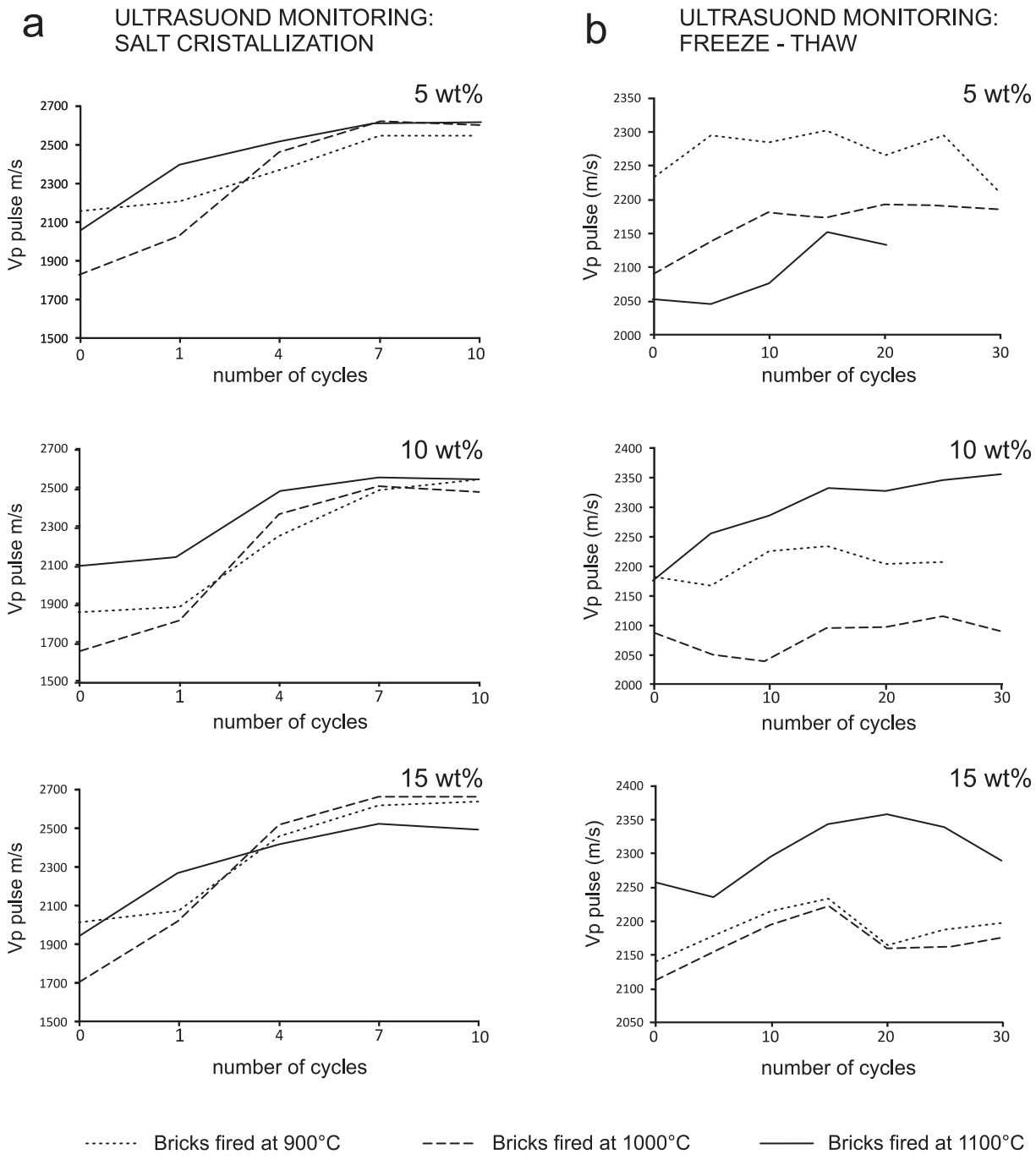

Fig. 10. a) Propagation velocities of ultrasonic Vp pulses (m s^{-1}) during salt crystallization test; b) propagation velocities of ultrasonic Vp pulses (m s^{-1}) during freeze–thaw test.

Table 7
Colorimetric parameters of dried and wet bricks. a^*: green-red chromatic coordinate; b^*: yellow-blue chromatic coordinate; L^*: lightness parameter; ΔE^*: total chromatic difference in dried and wet samples.

Sample		B5.09	B5.10	B5.11	B10.09	B10.10	B10.11	B15.09	B15.10	B15.11
Tr (wt%)		5			10			15		
T(°C)		900	1000	1100	900	1000	1100	900	1000	1100
Dry	a^*	15.05	16.58	13.35	14.45	14.53	12.96	15.48	16.03	12.73
	b^*	24.38	26.22	22.96	23.24	22.47	22.43	25.14	25.22	22.21
	L^*	58.38	58.49	57.82	61.34	58.89	54.88	61.12	60.23	53.39
Wet	a^*	17.89	18.85	16.03	17.42	17.95	15.08	18.99	19.05	14.35
	b^*	25.02	25.11	22.22	25.46	23.87	22.57	27.31	25.89	21.94
	L^*	44.65	44.1	42.63	46.37	45.63	42.45	46.4	45.27	42.25
	ΔE^*	14.04	14.61	15.44	15.42	13.77	12.61	15.29	15.28	11.26

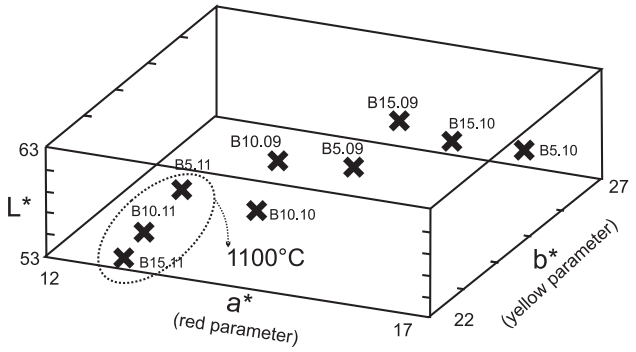

Fig. 11. Spectrophotometry: dried fired samples in L*a*b* space.

- as observed under SEM and confirmed by NA analysis, pore structure changes with increasing firing temperature and trachyte content, and pores become larger and rounder in shape;
- all the studied bricks display excellent physical and mechanical characteristics. In particular, uniaxial compressive strength is clearly correlated with firing temperature and trachyte content, together with increased compactness and vitrification;
- high trachyte contents (15 wt%) do not affect the thermal conductivity of bricks, since little differences can be observed with respects to the other mixes (5% and 10% of trachyte);
- all bricks have high resistance to decay in environmental conditions (freeze–thaw and salt crystallization) without substantial weight loss;
- brick color changes with firing temperature, acquiring darker hues at higher temperatures. Trachyte content has only a minor effect on the color of bricks, whether they are dry or wet. Therefore, trachyte waste in the range 5–15 wt% can be added without affecting aesthetic properties.

The good physical–mechanical performance characterizing all these materials indicates that, in brick production, trachyte waste represents an excellent alternative temper without affecting aesthetic features, thus fulfilling some market requirements for building materials with a traditional aspect. The re-use of trachyte waste may reduce requirements for some of the raw materials currently exploited. The fluxing effect of trachyte improves the physical and mechanical properties of bricks, so that high-quality products can be obtained already at a firing temperature of 900 °C and a trachyte concentration of 10 wt%, with the prospect of a lower firing temperature, thus reducing production costs and greenhouse gas emissions.

Acknowledgments

This study was funded by Research Group RNM179 of the Junta de Andalucía, Research Project MAT2016-75889-R, and overseas mobility grant 'Fondazione Ing. Aldo Gini'. Funding was also received from INPS - *Gestione Ex Inpdap (Direzione Regionale Veneto)* through the 'Doctor J' PhD grant for the period 2013-2015, and from the University of Padova (Research Project CPDA151883). The authors are grateful to the companies *SanMarcoTerreal Italia s.r.l.* and *Martini s.r.l.* for collaboration in providing materials and supporting technologies, and to Gabriel Walton who revised the English text.

References

[1] M. Dondi, M. Marsigli, B. Fabbri, Recycling of industrial and urban wastes in brick production – A review, Tile Brick Int. 13 (1997) 218–225.
[2] M. Dondi, M. Marsigli, B. Fabbri, Recycling of industrial and urban wastes in brick production – A review (Part 2), Tile Brick Int. 13 (1997) 302–309.
[3] I. Demir, Effect of organic residues addition on the technological properties of clay bricks, Waste Manage. 28 (2008) 622–627.
[4] S.P. Raut, R.V. Ralegaonkar, S.A. Mandavgane, Development of sustainable construction material using industrial and agricultural solid waste: A review of waste-create bricks, Constr. Build. Mater. 25 (2011) 4037–4042.
[5] L. Zhang, Production of bricks from waste materials – A review, Constr. Build. Mater. 47 (2013) 643–655.
[6] P. Muñoz Velasco, M.P. Morales Ortíz, M.A. Mendívil Giró, L. Muñoz Velasco, Fired clay bricks manufactured by adding wastes as sustainable construction material – A review, Constr. Build. Mater. 63 (2014) 97–107.
[7] S. Neves Monteiro, C.M. Fontes Vieira, On the production of fired clay bricks from waste materials: a critical update, Constr. Build. Mater. 68 (2014) 599–610.
[8] C. Bories, M.E. Borredon, E. Vedrenne, G. Vilarem, Development of eco-friendly porous fired clay bricks using pore-forming agents: a review, J. Environ. Manage. 143 (2014) 186–196.
[9] I. Demir, M.S. Baspınara, M. Orhan, Utilization of kraft pulp production residues in clay brick production, Build. Environ. 40 (2005) 1533–1537.
[10] M. Sutcu, S. Akkurt, The use of recycled paper processing residues in making porous brick with reduced thermal conductivity, Ceram. Int. 35 (2009) 2625–2631.
[11] D. Rajput, S.S. Bhagade, S.P. Raut, R.V. Ralegaonkar, S.A. Mandavgane, Reuse of cotton and recycle paper mill waste as building material, Constr. Build. Mater. 34 (2012) 470–475.
[12] M. Sutcu, J.J. del Coz Diaz, F.P. Alvarez Rabanal, O. Gencel, S. Akkurt, Thermal performance optimization of hollow clay bricks made up of paper waste, Energy Build. 75 (2014) 96–108.
[13] I. Demir, An investigation on the production of construction brick with processed waste tea, Build. Environ. 41 (2006) 1274–1278.
[14] K.Y. Chiang, P.H. Chou, C.R. Hua, K.L. Chien, C. Cheeseman, Lightweight bricks manufactured from water treatment sludge and rice husks, J. Hazard. Mater. 171 (2009) 76–82.
[15] D. Eliche-Quesada, F.A. Corpas-Iglesias, L. Pérez-Villarejo, F.J. Iglesias-Godino, Recycling of sawdust, spent earth from oil filtration, compost and marble residues for brick manufacturing, Constr. Build. Mater. 34 (2012) 275–284.
[16] C. Fernández-Pereira, J.A. de la Casa, A. Gómez-Barea, F. Arroyo, C. Leiva, Y. Luna, Application of biomass gasification fly ash for brick manufacturing, Fuel 90 (2011) 220–232.
[17] L. Pérez-Villarejo, D. Eliche-Quesada, Fco. J. Iglesias-Godino, C. Martínez-García, Fco. A. Corpas-Iglesias, Recycling of ash from biomass incinerator in clay matrix to produce ceramic bricks, J. Environ. Manage. 95 (2012) 349–354.
[18] L. Barbieri, F. Andreola, I. Lancellotti, R. Taurino, Management of agricultural biomass wastes: preliminary study on characterization and valorisation in clay matrix bricks, Waste Manag. 33 (2013) 2307–2315.
[19] D. Eliche-Quesada, S. Martínez-Martínez, L. Pérez-Villarejo, F.J. Iglesias-Godino, C. Martínez-García, F.A. Corpas-Iglesias, Valorization of biodiesel production residues in making porous clay brick, Fuel Process. Technol. 103 (2012) 166–173.
[20] İ.B. Topçu, B. Işidağ, Manufacture of high heat conductivity resistant clay bricks containing perlite, Build. Environ. 42 (2007) 3540–3546.
[21] B. Ercikdi, G. Külekci, T. Yilmaz, Utilization of granulated marble wastes and waste bricks as mineral admixture in cemented paste backfill of sulphide-rich tailings, Constr. Build. Mater. 93 (2015) 573–583.
[22] N. Bilgin, H.A. Yeprem, S. Arslan, A. Bilgin, E. Gunay, M. Marsoglu, Use of waste marble powder in brick industry, Constr. Build. Mater. 29 (2012) 449–457.
[23] M. Sutcu, H. Alptekin, E. Erdogmus, Y. Er, O. Gencel, Characteristics of fired clay bricks with waste marble powder addition as building materials, Constr. Build. Mater. 82 (2015) 1–8.
[24] B. Ercikdi, F. Cihangir, A. Kesimal, H. Deveci, I. Alp, Utilization of industrial waste products as pozzolanic material in cemented paste backfill of high sulphide mill tailings, J. Hazard. Mater. 168 (2009) 848–856.
[25] G. Cultrone, E. Sebastián, Fly ash addition in clayey materials to improve the quality of solid bricks, Constr. Build. Mater. 23 (2009) 1178–1184.
[26] L. Zhang, S. Ahmari, J. Zhang, Synthesis and characterization of fly ash modified mine tailings-based geopolymers, Constr. Build. Mater. 25 (2011) 3773–3781.
[27] A. Yagüe, S. Valls, E. Vázquez, V. Kuchinow, Utilización de lodo seco de depuradora de aguas residuales como adición en adoquines de hormigón prefabricado, Mater. Constr. 52 (267) (2002) 31–41.
[28] C.H. Weng, D.F. Lin, P.C. Chiang, Utilization of sludge as brick materials, Adv. Environ. Res. 7 (2003) 679–685.
[29] J.A. Cusidó, L.V. Cremades, Environmental effects of using clay bricks produced with sewage sludge: leachability and toxicity studies, Waste Manag. 31 (2012) 1372–1380.
[30] P.P. Manca, G. Orrù, P. Desogus, Recycling of sludge from ornamental stone processing as resource in civil constructions, Int. J. Min. Reclam. Environ. 29 (2015) 141–155.
[31] C. Coletti, L. Maritan, G. Cultrone, C. Mazzoli, Use of industrial ceramic sludge in brick production: effect on aesthetic quality and physical properties, Constr. Build. Mater. 124 (2016) 219–227.
[32] Y. Chen, Y. Zhang, T. Chen, Y. Zhao, S. Bao, Preparation of eco-friendly construction bricks from hematite tailings, Constr. Build. Mater. 25 (2011) 2107–2111.
[33] O. Ortiz, F. Castells, G. Sonnemann, Sustainability in the construction industry: a review of recent developments based on LCA, Constr. Build. Mater. 23 (2009) 28–39.
[34] S.K. Haldar, Mineral Exploration: Principles and Applications, Elsevier Science Publishing Co Inc, United States, 2013.

[35] C. Koroneos, A. Dompros, Environmental assessment of brick production in Greece, Build. Environ. 42 (2007) 2114–2123.
[36] E. Peris, Mora, Life cycle, sustainability and the transcendent quality of building materials, Build. Environ. 42 (2007) 1329–1334.
[37] Y. Asiedu, P. Gu, Product life cycle cost analysis: state of the art review, Int. J. Prod. Res. 36 (1998) 883–908.
[38] V. Bozkurt, A. Kara, Y. Uçbas, K. Kayaci, M. Çiftçi, Possible use of trachyte as a flux in floor tile production, Ind. Ceram. 26 (2006) 87–94.
[39] Y. Uçbas, V. Bozkurt, K. Bilir, Recovery of sanidine from trachyte, in: Proceedings of the 11th International Mineral Processing Symposium, Belek-Antalya, Turkey, 2008.
[40] A. Kara, K. Kayaci, A.S. KüçüKer, V. Bozkurt, Y. Uçbas, S. Özdamar, Use of rhyolite as flux in porcelain tile production, Ind. Ceram. 29 (2009) 71–81.
[41] L. Maritan, Corse Iron Age pottery from Este (Padova), Italy, Servicio de Publicaciones de la Universidad de Alcalá, 2001, pp. 1–6.
[42] L. Maritan, Archaeometric study of Etruscan-Padan type pottery from the Veneto region: petrographic, mineralogical and geochemical-physical characterisation, Eur. J. Mineral. 16 (2004) 297–307.
[43] L. Maritan, C. Mazzoli, M. Tenconi, G. Leonardi, S. Boaro, Provenance and production technology of Early Bronze Age pottery from a lake dwelling settlement at Arquà Petrarca (Padova, NE Italy), in: P.S. Quinn (Ed.), Interpreting Silent Artefacts: Petrographic Approaches to Archaeological Ceramics, Archaeopress, Oxford, 2009, p. 8199.
[44] M. Tenconi, L. Maritan, G. Leonardi, B. Prosdocimi, C. Mazzoli, Ceramic production and distribution in North-East Italy: study of a possible trade network between Friuli Venezia Giulia and Veneto regions during the final Bronze Age and early Iron Age through analysis of peculiar 'flared rim and flat lip' pottery, Appl. Clay Sci. 82 (2013) 121–134.
[45] V.D. Scott, G. Love, Quantitative Electron Probe Microanalysis, John Wiley and Sons, New York, 1983.
[46] G. Chen, J. Wang, The preparation of marine geological certified reference materials - polymetallic nodule GSPN-1 and marine sediment GSMS-1 from the Central Pacific Ocean, Geostand. Geoanal. Res. 22 (1998) 119–125.
[47] TOPAS version 4.1. Bruker AXS, Karlsruhe, Germany, 2007.
[48] UNI EN 13755, Natural stone test methods - Determination of water absorption at atmospheric pressure. CNR-ICR, Rome, 2008.
[49] RILEM, Recommended test to measure the deterioration of stone and to assess the differences of treatment methods. Matériaux et Constructions 13, 1980, 175–253.
[50] G. Cultrone, M.J. de la Torre, E. Sebastián, O. Cazalla, Evaluación de la durabilidad de ladrillos mediante técnicas destructivas (TD) y no-destructivas (TND), Mater. Constr. 53 (2003) 41–59.
[51] UNI EN 1925, Natural stone test methods - Determination of water absorption coefficient by capillarity. CNR-ICR, Rome, 2000.
[52] J. Guydader, A. Denis, Propagation des ondes dans les roches anisotropes sous contrainte évaluation de la qualité des schistes ardoisiers, Bull. Int. Assoc. Eng. Geol. 33 (1986) 49–55.
[53] UNI EN 1926, Natural stone test methods - Determination of uniaxial compressive strength, ICNR-ICR, Rome, 2007.
[54] A. Hein, N.S. Müller, P.M. Day, V. Kilikoglou, Thermal conductivity of archaeological ceramics: the effect of inclusions, porosity and firing temperature, Thermochim. Acta 480 (2008) 35–42.
[55] I. Allegretta, G. Eramo, D. Pinto, A. Hein, The effect of temper on the thermal conductivity of traditional ceramics: nature, percentage and granulometry, Thermochim. Acta 581 (2014) 100–109.
[56] UNI EN 12370, Natural stone test methods - Determination of resistance to salt crystallisation. CNR-ICR, Rome, 2001.
[57] UNI EN 12371, Natural stone test methods - Determination of frost resistance. CNR-ICR, Rome, 2010.
[58] UNI EN 15886, Conservation of cultural property - Test methods - Colour measurement of surfaces. CNR-ICR, Rome, 2010.
[59] L. Germinario, J.M. Hanchar, R. Sassi, L. Maritan, R. Cossio, A. Borghi, C. Mazzoli, New petrographic and geochemical tracers for recognizing the provenance quarry of trachyte of the Euganean Hills, northeastern Italy, Geoarchaeology (2017) 1–23.
[60] G. Cultrone, E. Sebastián, K. Elert, M.J. de la Torre, O. Cazalla, C. Rodriguez-Navarro, Influence of mineralogy and firing temperature in the porosity of bricks, J. Eur. Ceram. Soc. 34 (2004) 547–564.
[61] G. Cultrone, C. Rodríguez Navarro, E. Sebastián, O. Cazalla, M.J. de la Torre, Carbonate and silicate phase reactions during ceramic firing, Eur. J. Mineral. 13 (2001) 621–634.
[62] L. Maritan, L. Nodari, C. Mazzoli, A. Milano, U. Russo, Influence of firing conditions in ceramic products: experimental study on clay rich in organic matter, Appl. Clay Sci. 31 (2006) 1–15.
[63] C. Rodriguez-Navarro, G. Cultrone, A. Sanchez-Navas, E. Sebastián, TEM study of mullite growth after muscovite breakdown, Am. Mineral. 88 (2003) 713–724.
[64] G. Cultrone, E. Molina, A. Arizzi, The combined use of petrographic, chemical and physical techniques to define the technological features of Iberian ceramics from the Canto Tortoso area (Granada, Spain), Ceram. Int. 40 (2014) 10803–10816.
[65] I. Allegretta, D. Pinto, G. Eramo, Effects of grain size on the reactivity of limestone temper in a kaolinitic clay, Appl. Clay Sci. 126 (2016) 223–234.
[66] R.S. James, A.C. Turnock, J.J. Fawcett, The stability and phase relations of iron chlorite below 8.5 kb P-H_20, Contrib. Mineral. Petrol. 56 (1976) 1–25.
[67] G. Sedmale, I. Sperberga, U. Sedmalis, Z. Valancius, Formation of high-temperature crystalline phases in ceramic from illite clay and dolomite, J. Eur. Ceram. Soc. 26 (2006) 3351–3355.
[68] S. Kurama, H. Kurama, The reaction kinetics of rice husk based cordierite ceramics, Ceram. Int. 34 (2008) 269–272.
[69] P. Duminuco, B. Messiga, M.P. Riccardi, Firing process of natural clays. Some microtextures and related phase compositions, Thermochim. Acta 321 (1998) 185–190.
[70] M.P. Riccardi, B. Messiga, P. Duminuco, An approach to the dynamics of clay firing, Appl. Clay Sci. 15 (1999) 393–409.
[71] A.F. Gualtieri, Accuracy of XRPD QPA using the combined Rietveld–RIR method, J. Appl. Cryst. 33 (2000) 267–278.
[72] R. Sassi, C. Mazzoli, R. Spiess, T. Cester, Towards a better understanding of the fibrolite problem: the effect of reaction overstepping and surface energy anisotropy, J. Petrol. 45 (2004) 1467–1479.
[73] S.S. Singer, F. Singer, Industrial Ceramics, Chapman and Hall, London, 1963.
[74] B. Yoshiki, K. Matsumoto, High-temperature modification of barium feldspar, J. Am. Ceram. Soc. 34 (1951) 283–286.
[75] W.A. Deer, R.A. Howie, J. Zussman, Rock-Forming Minerals, Volume 4A: Framework Silicates – Feldspars, London, The Geological Society, 2001.
[76] D. Benavente, L. Linares-Fernández, G. Cultrone, E. Sebastián, Influence of microstructure on the resistance to salt crystallization damage in bricks, Mater. Struct. 39 (2006) 105–113.
[77] A. Salem, S. Aghahosseini, Determination of fluxing agents mixing ratio for enhancing thermal shock resistance of ceramic Raschig ring via systematic approach, Thermochim. Acta 545 (2012) 57–66.
[78] K.S.W. Sing, D.H. Everett, R.A.W. Haul, L. Moscou, R.A. Pierotti, J. Rouquérol, T. Siemienievska, Reporting physisorption data for gas/solid systems with special reference to the determination of surface area and porosity, Pure Appl. Chem. 57 (1985) 603–619.
[79] L.M. Anovitz, D.R. Cole, Characterization and Analysis of porosity and pore structure, Rev. Mineral. Geochem. 80 (2015) 61–164.
[80] J. Martínez-Martínez, D. Benavente, S. Ordóñez, M.A. García-del-Cura, Multivariate statistical techniques for evaluating the effects of brecciated rock fabric on ultrasonic wave propagation, Int. J. Rock Mech. Min. Sci. 45 (2008) 609–620.
[81] F. Cernuschi, S. Ahmaniemi, P. Vuoristo, T. Mäntylä, Modelling of thermal conductivity of porous materials: application to thick thermal barrier coatings, J. Eur. Ceram. Soc. 24 (2004) 2657–2667.
[82] J. García Ten, M.J. Orts, A. Sabutit, G. Silva, Thermal conductivity of traditional ceramics. Part I: Influence of bulk density and firing temperature, Ceram. Int. 36 (2010) 1951–1959.
[83] M. Karoglou, A. Moropoulou, A. Giakoumaki, M.K. Krokida, Capillary rise kinetics of some building materials, J. Colloid Interface Sci. 284 (2005) 260–264.
[84] C. Coletti, G. Cultrone, L. Maritan, C. Mazzoli, Combined multi-analytical approach for study of pore system in bricks: how much porosity is there?, Mater Charact. 121 (2016) 82–92.
[85] I. Johari, B.H. Abu Bakar, Z.A. Ahmad, Effect of the change of firing temperature on microstructure and physical properties of clay bricks from Beruas (Malaysia), Sci. Sinter. 42 (2010) 245–254.
[86] C.A. Rios, M.A. Ramos, E. Plaza, A comparative study of mineralogical transformations in fired clays from the Laboyos Valley, Upper Magdalena Basin (Colombia), Boletín de Geología 34 (2012) 1.
[87] D.L. Whitney, B.W. Evans, Abbreviations for names of rock-forming minerals, Am. Mineral. 95 (2010) 185–187.